Refereed Proceedings

The 13th International Conference on Fluidization - New Paradigm in Fluidization Engineering

Engineering Conferences International *Year* 2010

CFD SIMULATION OF PHARMACEUTICAL PARTICLE DRYING IN A BUBBLING FLUIDIZED BED REACTOR

Jungkee Jang* Cezar Rosa†
Hamid Arastoopour‡

*Illinois Institution of Technology
†Illinois Institution of Technology
‡Illinois Institute of Tech., arastoopour@iit.edu

CFD SIMULATION OF PHARMACEUTICAL PARTICLE DRYING IN A BUBBLING FLUIDIZED BED REACTOR

Jungkee Jang, Cezar Rosa, Hamid Arastoopour

Department of Chemical and Biological Engineering, Illinois Institution of Technology, USA

ABSTRACT

The bubbling fluidized bed flow regime is characterized by high heat and mass transfer rate and leads to a relatively short drying time. In this study, the gas-solid mixing and drying of pharmaceutical particles in a bubbling fluidized bed reactor was simulated using Computational Fluid Dynamics approach.

INTRODUCTION

Particle drying using batch fluidized bed system has great potential in pharmaceuticals, chemicals, and agricultural applications since it provides a number of advantages such as large heat capacity inside a bed, rapid heat and mass transfer rate and relatively short drying time. Szafran R.G. and Kmiec A. (4) studied CFD modeling of heat and mass transfer in a spouted bed dryer using FLUNET CFD software. The Eulerian – Eulerian multiphase model incorporated in computational fluid dynamics codes has been used to predict gas-solid flow behavior and mixing in fluidized bed system (3,5). These models have also been extended to simulate heat and mass transfer in fluidized bed. Behjat et al.(6) studied behavior of gas-solid fluidized beds with Eulerian-Eulerian model approach. The estimated time-average bed expansion ratio and cross-sectional void profiles were compared well with corresponding values of experimental data. Wang et al. (7) proposed a approach to investigate drying characteristic of batch fluidized bed dryer based on a three phase model and CFD simulation using FLUENT. They also used electrical capacitance tomography (ECT) to measure the moisture content of particles.

The purpose of this study is to simulate transport phenomena during drying process of pharmaceutical granules in a bubbling fluidized bed using CFD approach and to predict qualitative and quantitative behavior of the flow patterns and particle mixing and heat and mass transfer using FLUENT CFD code. The expressions of thermal conductivity, particle density, and drying rate were added in the form of an executable code by means of a user defined function (UDF) to the governing equations in FLUENT code. Moisture transfer in each phase was introduced using a user defined scalar transport equation (UDS).

CFD MODEL

The CFD model used in this work is based on a two fluid model (TFM) and the kinetic theory of granular flow to describe flow behavior in a bubbling fluidized bed. In TFM approach both phases are considered to be continuous and fully interpenetrating. A set of governing equations to describe the dynamics behavior, heat and mass transfer phenomena of drying process in a bubbling fluidized bed was

developed and solved using FLUENT 6.3. Table 1 shows continuity, momentum, and energy equations for each phase. To close the sets of governing equation, constitutive equations are needed. The empirical correlation introduced by Gunn (4) was used to calculate the heat and mass transfer between gas and particulate phase (see Table 3).
To describe the moisture transfer in gas phase and solid phase, species balance equations for each phase are applied and the equations are expressed as a user define scalar (UDS) in FLUENT 6.3;

$$\frac{\partial(\varepsilon_g \rho_g Y_v)}{\partial t} + \nabla \cdot (\varepsilon_g \rho_g \vec{v}_g Y_v) = \nabla \cdot (D_{v,g} \rho_v \varepsilon_g \nabla Y_v) + \dot{m} \qquad (1)$$

$$\frac{\partial(\varepsilon_s \rho_s X_s)}{\partial t} + \nabla \cdot (\varepsilon_s \rho_s \vec{v}_s X_s) = \nabla \cdot (D_{v,s} \rho_s \varepsilon_s \nabla X_s) - \dot{m} \qquad (2)$$

In this study, we assumed there is no water in outer particle surface since the external resistance has insignificant effect on drying process (4). Therefore, we only considered falling-rate period of drying model. To describe moisture transfer in a particle, we applied following diffusion model proposed by Crank (1) which is based on the analytical solution of Fick's diffusion equation for a spherical particle.

$$\dot{m} = \frac{D_{v,s} \pi^2 \rho_{s,d} \varepsilon_s}{R^2} (X_m - X_{m,e}) \qquad (3)$$

The governing equations in Table 1 along with constitutive equations in Table 2 and species balance equations were solved using FLUENT6.3. To reduce computational time, we assumed 2-D axial symmetric bed. Figure 1 shows the computational geometry with much finer computational cell in the region of the bed which contained particles. Pressure-velocity coupling was applied using the SIMPLE algorithm. The first-order upwind discretization method was used for governing equations and convergence criterion of simulations was considered less than 0.0001.

The boundary conditions for the gas/solid phases are summarized as following: i) heat transfer from wall of the heat to surrounding was neglected, and partial slip condition which is non-slip condition for gas phase and free slip condition for solid phase was assumed. ii) Inlet condition was treated as a velocity inlet boundary condition with uniform velocity distribution. iii) In the outlet, pressure boundary condition was applied. iv) Axial symmetry boundary condition was considered along the axis. The flow and heat transfer properties and inlet and outlet conditions are summarized in Table 3.

RESULTS AND DISCUSSION

Grid-Size Independency Test

To obtain accurate and meaningful simulation results, calculated values should be independent of grid size. Therefore, simulations were carried out using three different numbers of meshes to investigate grid size effects (see Table 4). To prove grid independency of numerical results, power spectrum analysis was used. In this study, fluctuation of solid volume fraction was detected at three different positions, bed height, z=3cm, 6cm, and 9cm with the same radial position, r=3cm. After obtaining time domain values for solid volume fraction fluctuation, time domain values were calculated to frequency domain data using Fast Fourier Transform (FFT). The dominant frequency is 3.2 for all the three case and case B and C should have almost identical profile in power spectrum analysis. This means that the numerical results will not be different from each other with further increase in the number of grids from case B to C. Therefore, case B with less computational mesh was chosen for our simulations.

Table1. Governing equations for TFM model

Continuity equation

Gas phase

$$\frac{\partial}{\partial t}(\varepsilon_g \rho_g) + \nabla \cdot (\varepsilon_g \rho_g \vec{v}_g) = \dot{m}$$

Solid phase

$$\frac{\partial}{\partial t}(\varepsilon_s \rho_s) + \nabla \cdot (\varepsilon_s \rho_s \vec{v}_s) = -\dot{m}$$

Conservation of momentum

Gas phase

$$\frac{\partial(\varepsilon_g \rho_g \vec{v}_g)}{\partial t} + \nabla \cdot (\varepsilon_g \rho_g \vec{v}_g \vec{v}_g) = -\varepsilon_g \nabla p + \nabla \cdot \bar{\bar{\tau}}_g + \varepsilon_g \rho_g g + K_{gs}(\vec{v}_g - \vec{v}_s)$$

Solid phase

$$\frac{\partial(\varepsilon_s \rho_s v_s)}{\partial t} + \nabla \cdot (\varepsilon_s \rho_s \vec{v}_s \vec{v}_s) = -\varepsilon_s \nabla p - \nabla p_s + \nabla \cdot \bar{\bar{\tau}}_s + \varepsilon_s \rho_s g + K_{sg}(\vec{v}_s - \vec{v}_g)$$

Conservation of thermal energy equation

Gas phase

$$\frac{\partial(\varepsilon_g \rho_g h_g)}{\partial t} + \nabla \cdot (\varepsilon_g \rho_g \vec{u}_g h_g) = -\varepsilon_g \frac{\partial p_g}{\partial t} + \bar{\bar{\tau}}_g : \nabla \vec{u}_g - \nabla \cdot \vec{q}_g + Q_{sg} + \dot{m} \Delta H_{vap}$$

Solid phase

$$\frac{\partial(\varepsilon_s \rho_s h_s)}{\partial t} + \nabla \cdot (\varepsilon_s \rho_s \vec{u}_s h_s) = -\varepsilon_s \frac{\partial p_s}{\partial t} + \bar{\bar{\tau}}_s : \nabla \vec{u}_s - \nabla \cdot \vec{q}_s + Q_{gs} - \dot{m}_{pq} \Delta H_{vap}$$

Granular temperature equation

$$\frac{3}{2}[\frac{\partial}{\partial t}(\rho_s \varepsilon_s \theta_s) + \nabla \cdot (\rho_s \varepsilon_s \vec{v}_s \theta_s)] = (-p_s \bar{I} + \bar{\bar{\tau}}_s) : \nabla \cdot \vec{v}_s + \nabla \cdot (k_{\theta_s} \nabla \theta_s) - \gamma \theta_s + \phi_{gs}$$

Table 2 Constitutive Relations for TFM Model

Stress-strain tensor for gas phase

$$\tau_g = 2\varepsilon_g \mu_g \{\frac{1}{2}(\nabla u_g + \nabla u_g^T) - \frac{1}{3}(\nabla \cdot u_g)\bar{I}\}$$

Stress-strain tensor for solid phase

$$\tau_s = (-p_s)\bar{I} + 2\mu_s \{\frac{1}{2}(\nabla u_s + \nabla u_s^T) - \frac{1}{3}(\nabla \cdot u_s)\bar{I}\}$$

Solid pressure

$$p_s = \varepsilon_s \rho_s \theta_s + 2\rho_s (1 + e_{ss}) \varepsilon_s^2 g_o \theta_s$$

Drag coefficient

$$K_{gs} = \frac{3\varepsilon_s \varepsilon_g \rho_g}{4 v_{r,s}^2 d_s} C_D\left(\frac{\mathrm{Re}_s}{v_{r,s}}\right)\left|\vec{v}_s - \vec{v}_g\right|$$

$$v_{r,s} = 0.5[A - 0.06\,\mathrm{Re}_s + \sqrt{(0.06\,\mathrm{Re}_s)^2 + 0.12\,\mathrm{Re}_s(2B - A) + A^2}$$

$$A = \varepsilon_g^{4.14} \quad B = 0.8\varepsilon_g^{1.28} \quad \varepsilon_g \le 0.85 \; or \; B = \varepsilon_g^{2.65} \quad \varepsilon_g > 0.85$$

Solid shear viscosity

$$\lambda_s = \frac{4}{3_s}\,\varepsilon_s \rho_s d_s g_o (1 + e_{ss})\left(\frac{\theta_s}{\pi}\right)^{1/2}$$

Frictional solid viscosity

$$\mu_{s,fr} = \frac{p_s \sin\phi}{2\sqrt{I_{2D}}}$$

Granular temperature conductivity

$$k_{\theta_s} = \frac{15 d_s \rho_s \alpha_s \sqrt{\theta_s \pi}}{4(41 - 33\eta)}[1 + \frac{12}{5}\eta^2(4\eta - 3)\alpha_s g_o + \frac{16}{15\pi}(41 - 33\eta)\eta\alpha_s g_o)], \quad where\ \eta = 0.5(1 + e_{ss})$$

Granular energy exchange between phases

$$\phi_{gs} = -3k_{gs}\theta_s$$

Specific enthalpy of phase q

$$h_q = \int Cp_q dT_q$$

Volumetric inter-phase heat transfer coefficient

$$Q_{sg} = -Q_{gs} = \frac{\varepsilon_g}{d_s} h_{sg}(T_g - T_s)$$

$$Nu = \frac{h_{gs} d_s}{k_g} = (7 - 10\varepsilon_g + 5\varepsilon_g^2)(1 + 0.7\,\mathrm{Re}^{0.2}\,\mathrm{Pr}^{1/3}) + (1.33 - 2.4\varepsilon_g + 1.2\varepsilon_g^2)\,\mathrm{Re}^{0.7}\,\mathrm{Pr}^{1/3}$$

$$\mathrm{Re} = \frac{\rho_g U_0 d_s}{\mu_g} \qquad \mathrm{Pr} = \frac{Cp_g \mu_g}{k_g}$$

Latent heat due to vaporization for water

$$H_{vap} = 3168 - 2.4364T$$

Table3. Flow and heat and mass transfer properties, initial and inlet conditions

Particle size	225μm
Particle density	1200kg/m^3
Gas density	1.225kg/m^3
Gas viscosity	1.789*10^{-5}kg/m.s
Initial bed height	0.12m
Initial particle volume fraction	0.63
Inlet gas velocity	1.2m/s (0.006m^3/s)
Terminal gas velocity	2.03m/s
Minimum fluidized gas velocity	0.143m/s
Inlet gas temperature	378k
Initial solid temperature	298k
Initial moisture content	0.2kg$_{water}$/kg$_{dry\ solid}$
Equilibrium moisture content	0.002kg$_{water}$/kg$_{dry\ solid}$

Table4. Different number of meshes

Case	Number of meshes
A	24*15 and 68*15, total number of mesh=1390
B	42*30 and 44*30, total number of mesh=2550
C	50*40 and 52*40 , total number of mesh=4080

Hydrodynamic Behavior

To obtain better understanding of heat and mass transfer, we must simulate gas/solid flow to gain more knowledge of mixing and bubble formation in a bubbling bed. Simulations were run for 4s and the contour of solid volume fraction during 4s is shown on Figure 2. From Figure 2, first bubble was created around 0.2s and was broken around 0.4s at the top of the bed. To analyze solid mixing within the bed with respect to the two-phase model, it is important to understand the bubble wake. Since the bubble wake plays a major role on particle conveyance. This is a region of higher upward solid flux than the rest of the bed.

Figure 3 shows the contour plot for the solid flux and a well-defined bubble wake. Comparing the relative locations of upwards solid flux with that of the bubbles, we can see that the wakes are suited where expected, directly below the rising gas bubbles. By identifying the bubble wake, the circulation mechanism becomes clear. The wake follows the bubble upward through the bed, and is eventually deposited on the bed surface when bubble erupts. However, this bubble wake is constantly and apparently rapidly, mix with the solids in the bulk phase. Since exchange is simply particles moving into and out of the wake, the horizontal component of the solid flux may be used to show this mechanism. The vector plot for axial solid velocity demonstrates regions of solids moving into the wake from either side of the bubbles. The vector showing solids entering and exiting the wake, corresponding to the capturing and sloughing off of particles by the bubble wake.

Heat and Mass Transfer during Drying Process

Figure 4 shows contour plot of the instantaneous temperature distributions for each phase. In Figure 4, solid temperature is uniformly distributed in the entire bed. The rising bubbles yield a large solid particle replacement in the back of the bubble. This enhances solid circulation. Hence, cold particle are dragged into the back of the bubbles and raise the temperature gradient between cold and hot particles. Figure 5 presents the solid volume fraction and heat transfer coefficient obtained at radial position at different height at the 10 seconds. Heat transfer coefficient was observed from 0.475 W/m^2K to 0.250 W/m^2K. The profile of heat transfer coefficient is very similar to solid volume fraction, which means the bubble behavior plays a pivotal role in heat transfer between solid phase and gas phase. As bubble rise in the bed, the heat transfer coefficient is enhanced in the back of the bubble region. While bubbles are rising, coalescing, and breaking up, thermal energy is diffused through the bed, making the temperature more uniform.

Figure 6 shows averaged moisture mass fraction changes in solid phase which means how much moisture is evaporated from solid phase. Due to uniform solid mixing and temperature distribution in the bed, moisture is almost uniformly evaporated from solid phase. Because mass transfer process is very slow process, only 0.4% of moisture was transferred to gas phase for 12s. Figure 7 shows the variation of between the averaged moisture and temperature of solid phases with respect to time. This figure clearly shows continuous increase in particle temperature and continuous decrease in average

moisture content of particles. With temperature increasing, moisture content in solid phase keeps decreasing, which means that some part of the convective heat flux from air is used to evaporate the water.

CONCLUSION

CFD along with drying kinetic model and energy equation is very comprehensive approach in simulating drying process in fluidized bed system. This approach allows for description of the complex issues of coupled heat and mass transfer during drying process. It provides the transient flow patterns and particle mixing as well as the distributions of qualitative parameters in a fluidized bed. The predicted hydrodynamics behavior in a bed has an effect on the instantaneous distributions of the particle and gas temperature and the moisture removal from particles.

ACKNOWLEDEMENT

This work was financed by The National Institute for Pharmaceutical Technology and Education (NIPTE).

NOMENCLATURE

ds	Particle diameter, m	*Pr*	Prentle Number
D_v	Vapor diffusion coefficient, m^2/s	$\vec{v}$	Velocity, m/s
g	Gravity, m/s^2	X_m	Dry base moisture content in solid phase, $kg_{water}/kg_{dry\ solid}$
h	Heat transfer coefficient, W/m^2s	$X_{m,e}$	Equilibrium moisture content in solid phase, $kg_{water}/kg_{dry\ solid}$
K	Drag coefficient	X_s	Vapor fraction in solid phase, kg/kg
$\dot{m}$	Drying rate, kg/m.s	Y_v	Vapor fraction in air phase, kg/kg
Nu	Nusselt number	ρ	Density, kg/m^3
θ	Granular temperature, m^2/s^2	*Subscript*	
p	Pressure, Pa	*d*	Dry base
p_s	Solid pressure	*s*	Solid phase
$\vec{q}$	Convective heat transfer coefficient, W/m.s	*g*	Gas phase
R	Solid diameter, m	*vap*	Vapor phase
Re	Reynolds number		

REFERENCE

1. Crank, J., 1975. The mathematics of Diffuision,2nd ed. Clearendon Press,Oxford, U.K
2. Gunn, D.J., 1978. Transfer of Heat or Mass to Particles in Fixed and Fluidised Beds. *Int. J. Heat Mass Transfer*, 21, 467-476
3. Arastoopour, H.,2001. Numerical Simulation and Experimental Analysis of Gas/Solid Flow System. Powder Technology Journal, 119, 59-67
4. Szafran, R. G., Kmiec, A., 2004. CFD modeling of heat and mass transfer in a spouted bed dryer. Ind. Eng. Chem. Res. 78, 1025 – 1031
5. Dokka, S., and Arastoopour, H., 2007. Simulation of a Pulsating Bed Using Eulerian Approach. Fluidization XII, ECI, New York, 743-750

6. Behjat, Y., Shahhosseini, S., Hashemabadi, S.H., 2008. CFD modeling of hydrodynamic and heat transfer in fluidized bed reactors. International Communications in Heat and Mass Transfer 35,357-368
7. Wang, H.G., Yang, W.Q., Senior, P., Raghavan, R.S., Duncan, S.R., 2008. Investigation of batch fluidized bed drying by mathematical modeling, CFD simulation and ECT measurement. AIChE-J 54(2), 427-444

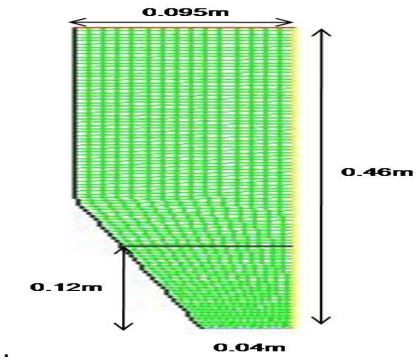

Figure1. Computational geometry

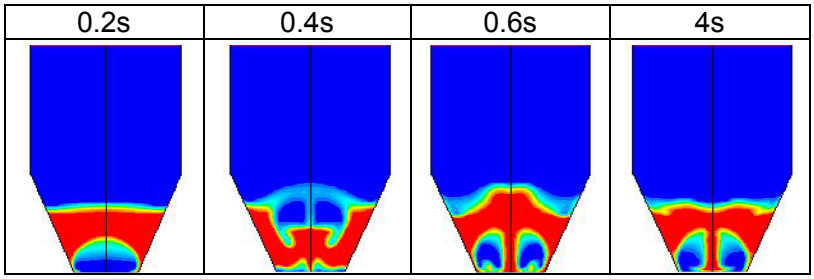

Figure2. Contour plot of solid volume fraction at different time

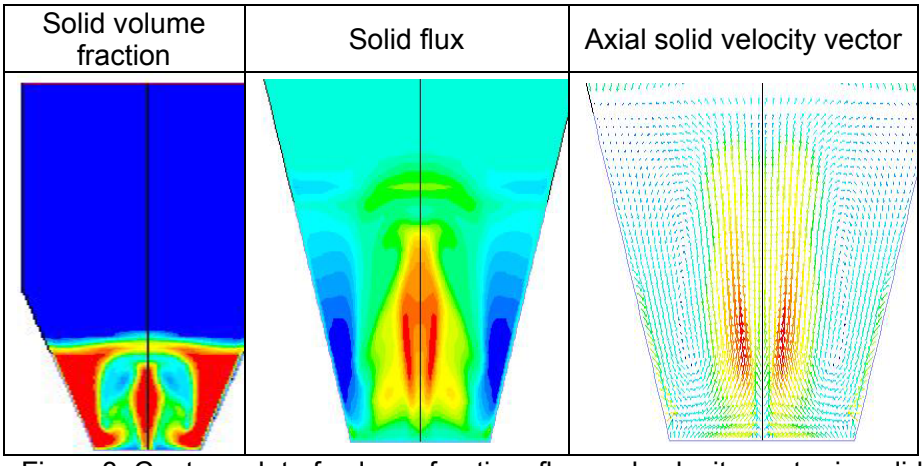

Figure3. Contour plot of volume fraction, flux and velocity vector in solid phase

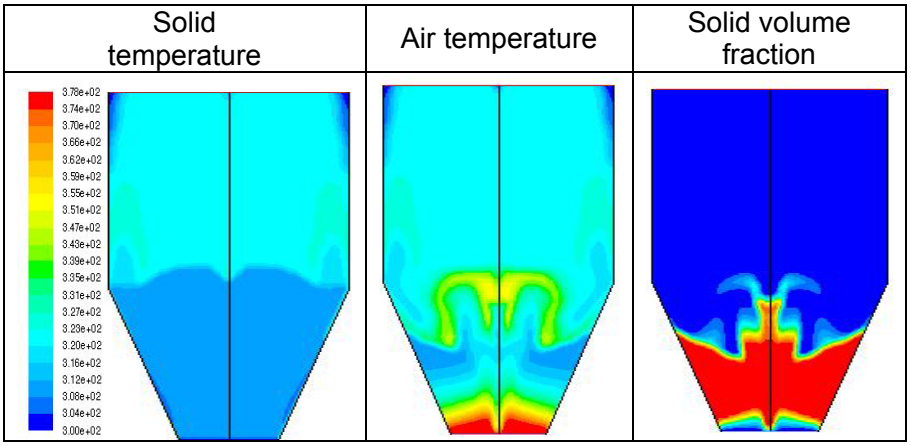

Figure4. Contour plot of temperature and volume fraction

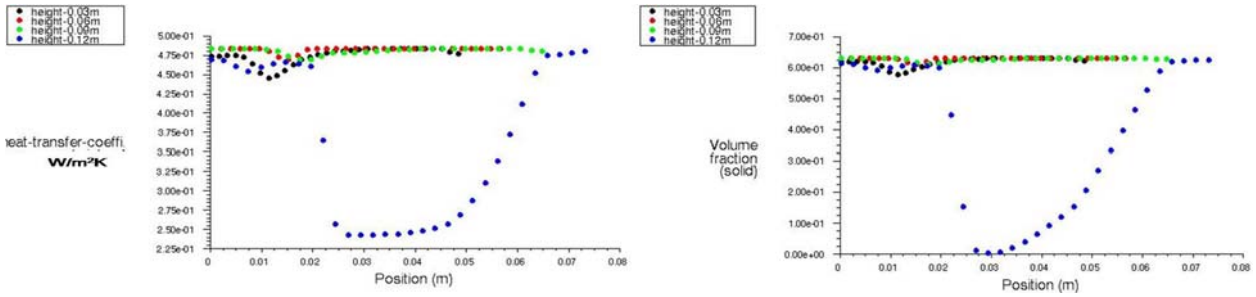

Figure5. The relationship between heat transfer coefficient and solid volume fraction

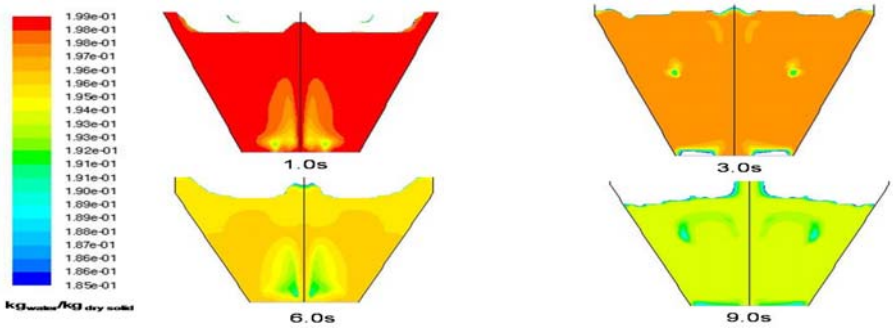

Figure6. Moisture mass fraction in solid phase

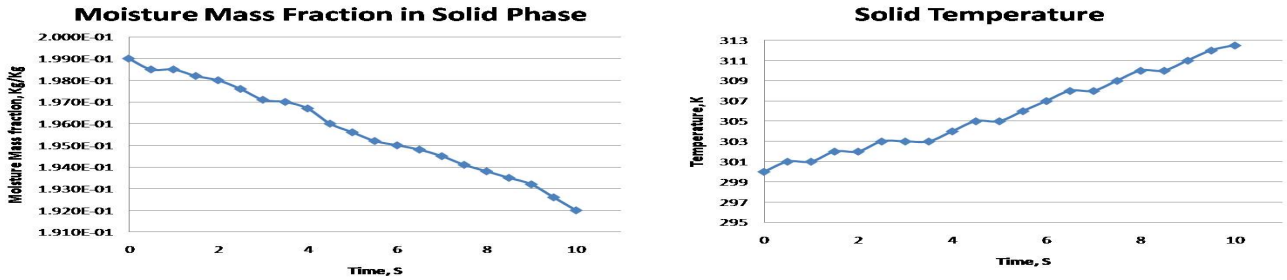

Figure7. The relationship between moisture mass fraction and temperature in solid phase